International Journal of GEOMATE, April, 2026 Vol.30, Issue 140, pp.44-55
ISSN: 2186-2982 (P), 2186-2990 (O), Japan, DOI: https://doi.org/10.21660/2026.140.5355
Geotechnique, Construction Materials and Environment

EFFECT OF GEOGRID REINFORCEMENT ON FLEXIBLE PAVEMENT PERFORMANCE OVER WEAK SUBGRADE UNDER DIFFERENT LOAD CONDITIONS

*Nawal D. Salman[1], Hasan H. Joni[2]

[1,2] Department of Highway and Geotechnical Engineering, College of Civil Engineering, University of Technology, Iraq

*Corresponding Author, Received: 27 Nov. 2025, Revised: 26 Jan. 2026, Accepted: 02 Feb. 2026

ABSTRACT: Flexible pavement constructed over a weak subgrade is subject to premature failure, such as severe rutting, cracking, and a high level of tensile strain at the bottom of the asphalt layer, which affects pavement service life. To overcome such issues, geogrid material is used to reinforce pavement layers. Most laboratory studies are limited to single load or static load conditions that provide insufficient explanation for pavement response under repeated dynamic loads. In this study, the responses of flexible pavement reinforced with biaxial and triaxial geogrid were evaluated using a laboratory 1/3 scale accelerated testing device at three loading scenarios (5, 6.5, and 7.5 KN). Five pavement sections were tested: control (unreinforced), triaxial and biaxial geogrid reinforcement at the middle of the subbase course layer, and at the subbase-subgrade interface. The surface rutting and tensile strain at the bottom of the asphalt layer were measured to evaluate the effect of reinforcement type and location. Results revealed that geogrid reinforcement, especially triaxial geogrid when placed at the subbase-subgrade interface, can significantly minimize rutting depth and tensile strain at the bottom of the asphalt layer. Triaxial geogrid at the interface reduced rutting by an average percent of 45%, tensile strain at the bottom of the asphalt layer by 84% relative to the control section, and a Traffic Benefit Ratio (TBR) of 4.0-4.3 corresponding to 303-326% improvement of load repetition.

Keywords: Flexible Pavement; Geogrid Reinforcement; Weak Subgrade; Accelerated Load Test; Rutting: TBR.

1. INTRODUCTION

A low bearing capacity of weak subgrade in flexible pavements often causes excessive deformation and premature failure, resulting in a reduction in the service life of the pavement [1]. In most cases, flexible pavements are constructed on weak subgrade soils. Their performance is significantly affected by the quality of the supporting subgrade. This issue is exacerbated by the limited natural resources of high-quality natural raw materials consumed by growing infrastructure and the gradual degradation of pavement material caused by overloading conditions that usually occur in developing countries [2-3]. As traffic volume and over axle loads imposed on pavements continuously increase, the need to improve pavement structural integrity has arisen [4].

In pavement construction, geogrid material is adopted as reinforcement for weak subgrade to overcome these issues [5-7]. Generally, geogrid materials improve bearing capacity and the efficiency of load distribution through the confinement mechanism. various studies have shown that incorporating geogrid within pavement layers at the base-subgrade interface can significantly improve structural capacity for subgrade soil, particularly when the subgrade is classified as weak soil [5-12]. It has been documented that reinforced pavement could reduce stress and strain on the subgrade layer, which minimizes the failure potential [13]. However, the performance of the geogrid materials depends highly on their properties, loading conditions, reinforcement location, and the interaction between geogrid ribs and aggregate particles surrounding them [14]. Several studies confirm that using geogrid in subgrade reinforcement for the flexible pavement system could effectively minimize granular base thickness, increase pavement service life, and reduce costs [15-18]. According to Kwon and Tutumlure (2011), the type and strength-stiffness characteristics of the geosynthetic reinforcement, as well as the strength of the aggregate and subgrade material, determine the necessary thickness of the aggregate layer [19]. Kim and Lee (2013) investigated flexible pavement systems and found that geogrid reinforcement led to a decrease of 68 % in tensile strain at the bottom of the asphalt layer and an 18 % decrease in the vertical strain at the top of the subgrade, indicating its effect in controlling both structural and functional behavior of the material [20]. In addition, large-scale laboratory testing has demonstrated that geogrid reinforcement may redistribute loads, and the reduction in vertical strains may be significant in weak subgrades [21]. Biaxial polypropylene or polyester geogrids are usually used in granular base reinforcement, showing an increase in the modulus and confinement effect [22]. Additionally, triaxial

geogrids exhibit multi-directional tensile stiffness when compared to biaxial geogrids, due to their triangular aperture geometry, which provides more uniform stress distribution and improves interlock with aggregate particles in pavement layers. This study extends the application of triaxial geogrids to scaled dynamic repeated load tests. Field tests and full-scale accelerated load tests (ALT) have shown that geogrids can enhance the performance of reinforcement flexible pavement, even though they are costly and time-consuming. Al-Qadi et al. (2011) presented results from ALT sections instrumented with more than 170 sensors and showed that while geogrid reinforcement resulted in reduced lateral deformation in the base layer, overall structural performance was enhanced [23]. Nevertheless, the availability of full-scale accelerated load test facilities is limited, particularly in developing countries. Scaled ALT tests under laboratory conditions are a useful alternative for simulating traffic loads and observing the mechanical response, and for verifying the benefits derived from the presence of geogrid reinforcement [23]. Although the reinforced benefits of geosynthetic materials have been widely reported, few studies have evaluated their performance under locally manufactured, scaled ALT conditions that simulate overload effects. This study conducted ALT tests to evaluate rutting and tensile strain responses under different load levels. Laboratory testing generally employs a single load magnitude, single axle pressure, or a single frequency (e.g., 550 kPa at 1 Hz or a 0.77 Hz cyclic plate load). Therefore, the objective of this research is to investigate the effect of geogrid (biaxial and triaxial) as subbase reinforcement on the response of flexible pavement placed over weak subgrade, under three load scenarios: one normal loading condition and two overloading conditions applied via a laboratory accelerated load test. This study introduces a manufactured accelerated load test with a 1/3 scale at the University of Technology in Iraq, due to the unavailability of full-scale accelerated load test equipment. Generally, small-scale models offer size reduction, simplicity, repeatability, test condition control, and cost-effectiveness [24] and provide realistic stress distribution and cumulative damage by load applied by a wheel that a plat load cannot accurately simulate. Additionally, when compared to numerical FEM analysis, it provides direct measurements for model responses that can be used in validation [4; 25;26]. The 1/3-scale Accelerated Loading Test (ALT) in this study incorporates triaxial geogrid with controlled weak subgrade and variable overload conditions a combination not previously examined in laboratory or field conditions according to Iraqi standards. Its hypothesis that triaxial geogrid could perform better than biaxial geogrid in terms of rutting and tensile strain at the bottom of the asphalt layer.

2. RESEARCH SIGNIFICANCE

This study presents a novel experimental evaluation of the performance of flexible pavement reinforced with biaxial and triaxial geogrid under different load conditions using a (1/3) scale Accelerated Load Test system developed locally in Iraq, by simulating realistic traffic conditions into scaled dynamic loading. This work evaluates rutting and tensile strain that support the development of cost-effective, locally applicable pavement reinforcement for developing countries.

3. MATERIALS AND METHODS

3.1 Subgrade Soil

The subgrade was clay soil collected from a local construction site near Baghdad, Iraq. It is classified as an A-7 soil by the AASHTO, with a group index of 88.2, and as a lean clay soil (CL) with low plasticity by the Unified Soil Classification System (USCS), with a low plasticity index of 23.36% and a liquid limit of 42.86%. Figure 1 shows the grain size distribution curve of the subgrade material. The specific gravity (Gs) was 2.690, with an optimum moisture content of 16.8%. A CBR (ASTM D1833-87) was conducted to investigate the subgrade soil strength, the test result of35.1% CBR ratio. To set the lifted subgrade soil at a low CBR, the unsoaked CBR was examined at various water contents to select the worst conditions that resulted in a low CBR. To achieve this, an unsoaked California bearing ratio (CBR) testing procedure was developed and implemented. It is crucial to note that the moisture content was increased to generate weak subgrade soil; hence, soil was compacted at a level more than the ideal water content of 26%, resulting in a CBR value of 2.1%.

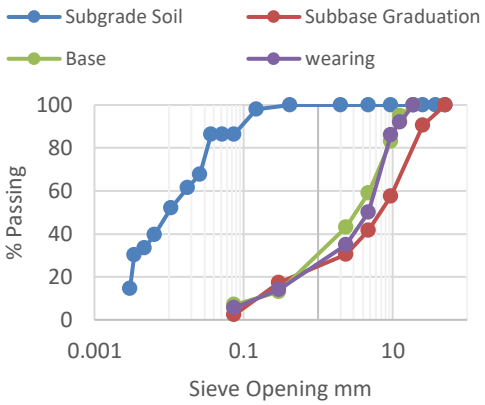

Fig. 1 Particle Size Distribution for pavement layers

3.2 Subbase Material

The subbase material used in this study was acquired from the Al-Ubaidei asphalt plant in Baghdad. Sieve analysis revealed a type B subbase gradation in accordance with the State Organization of Roads and Bridges' Standard Specification for Roads and Bridges in Iraq (SCRB, 2003), with a coefficient of uniformity (Cu) equal 83.3 and coefficient of curvature (Cc) equal 1.01, and D50 equal to 7 mm. This type is usually used in Iraq due to its availability and excellent drainage properties and bearing capacity suitable for the subbase layer. Standard laboratory tests were performed on the subbase materials to check their properties. The standard compaction test resulted in a maximum dry unit weight of 2.5 g/cm^3 in an optimum moisture content of 6%. The subbase material had a liquid limit of 22% and a specific gravity of 2.57. The CBR ratio with compaction to 95% of the maximum dry density was 35.1%. Table 1 lists the mechanical and physical characteristics of the material along with the relevant requirements.

3.3 Wearing Course and Bituminous Base Material

Al-Dura Refinery in Baghdad supplied the asphalt binder, which was utilized to construct the asphalt concrete mixture for the bituminous base and wearing surface course. The tests for physical properties of the binder result in a (40-50) grade asphalt, 113 cm ductility, 55 °C softening point, loss on heating 0.27, flash and fire point were (294 and 307 °C), rotational viscosity of 0.481 Pa.s at 135 °C and 0.122 Pa·s at 165 °C. this binder used to prepare wearing course layer and bituminous base course layer for the test models.

Marshall Mix Design procedure had been used to produce a hot bituminous stabilized base mixture and wearing course mixture in compliance with the SCRB Iraqi standards specification. The range of 3.0-5.5 percent for the base material was met by the asphalt mixture's 3.7% asphalt composition. Table 2 shows that the Marshall mixes had an appropriate flow of 3.1 mm and stability of 9.4 kN. The volumetric characteristics included 71.5% VFB, 14.4% VMA, and 4.1% air voids. To determine whether the aggregate used in this layer is suitable for pavement construction, it is subjected to a deleterious test and a soundness test using MgSO4. The results were 1.29% and 0.0705% for the former and latter, respectively, both of which met the standards listed in Table 2. In contrast, the hot-wearing course mixture was used as a surface layer for the test models, which were prepared using the Marshall mix design approach.

The asphalt content of the design mixture was 4.8%, which satisfies the 4.0–6.0% range for wearing coarse. As shown in Table 2, the Marshall mixes exhibited a stability of 10.1 kN and an acceptable flow of 3.3 mm. The voids in mineral aggregate were 15.5 %, the voids filled with binder were 73.5%, and the air voids were 4.1%. soundness test for aggregate used in wearing course mixture using MgSO4 revealed a value of 0.121%, and deleterious material was 1.314%; all the tests were within the required standards.

3.4 Geogrid Material

Geogrid material was supplied by Shandong XiuHe Engineering Materials Co., Ltd. in China. This study used two types of geosynthetic materials: PP biaxial geogrid BX3030 and PP triaxial geogrid TX150. Polyester biaxial geogrid is manufactured from high-tenacity multifilament polyester yarns and coated with a durable polymer. In contrast, PP triaxial geogrid TX150 is manufactured from select grades of High-Density Polyethylene through extruding and longitudinal stretching processes. It was made with a hexagonal shape and three-directionally arranged ribs. Consequently, ribs with rectangular cross-sections created the triangular apertures. Figure 2 shows the geogrid types used, and Table 3 illustrates specifications of the geogrids used in this study, provided by the manufacturing company. The geogrids were installed at two locations within the pavement model: In the middle depth of the subbase layer and at the subbase – subgrade interface.
According to Han et al (2018) the interaction between the geogrid and aggregate could be increased if the ratio of A/Dis suitable, where A is the geogrid opening size, and D is the effective aggregate size [27]. The reference specified the optimum range for biaxial geogrid by (1.30-1.71) and for triaxial geogrid by (1.08-1.43) [27]. For this study, the opening size of the geogrid is compatible with the aggregate size, where the ratio of A/D is equal to 1.42 for the biaxial geogrid and equal to 1.57 for the triaxial geogrid.

4. PAVEMENT MODEL DESIGN AND CONSTRUCTION

4.1 Experimental Setup

In this study, the experimental setup and scaled models utilized a 1/3 physical scale model to simulate the structural responses of a flexible pavement under repetitive axle loads. The full-scale pavement prototype chosen from the structural design for Iraqi Express No. 1 has a wearing surface of 4 cm, a binder course of 8 cm, a bituminous base of 20 cm, a subbase of 25 cm, and a subgrade thickness of 150 cm. Layers of 5.0 cm asphalt, 6.0 cm bituminous base, 9.0 cm subbase, and 50.0 cm subgrade were used to make the equivalent scaled model, which had a total thickness of 70 cm. A rubber tire with an exterior diameter of 30.5 cm was used to represent the load applied for the

Table 1. Iraqi Standards for wearing, Base, and Subbase coarse aggregate gradation (SCRB, 1983-R6)

Sieve Size "mm"	Sieve No. "inch"	Aggregate Material Gradation					
		Wearing Course		Base course		Subbase Course	
		Iraqi Standards Passing %	Blending %	Iraqi Standards Passing %	Blending %	Iraqi Standards Type B	Passing %
50.8	2	----	----	----	----	100	100
37.5	1.5			100	100	75-95	90.6
25	1			90-100	95	----	----
19	¾			76-90	83	----	----
12.5	½	100	100	56-80	68	----	----
9.5	3/8	80-100	88	48-74	61	40-75	57.5
4.75	No. 4	46-76	60	29-59	44	30-60	41.5
2.36	No. 8	28-58	41	19-45	32	21-47	30.5
0.3	No. 50	8-24	17	(5-17)	11	14-28	17.2
0.075	No. 200	4-12	9	(2-8)	5	5-15	2.3

Table 2. Stabilized Base Course and Surface Wearing Coarse Properties

Properties	Base		Wearing course	
	Result	Specification	Result	Specification
Asphalt (%) (40-50) Penetration	3.7	3.0 - 5.5	4.8	4.0-6.0
Stability (kN)	9.4	Min. 5	10.10	Min. 8
Flow (mm)	3.1	2 – 4	3.3	2 – 4
VTM (%)	4.1	3 – 6	4.1	3 – 5
VMA (%)	14.4	-----	15.5	-----
VFB (%)	71.5	-----	73.5	70-85
Density (g/cm^3)	2.311	-----	2.307	-----
Deleterious Material (%)	1.29	Max. 3	1.314	Max. 3
Soundness MgSo4 (%)	0.0705	Max. 18	0.121	Max. 18

tests. The prototype of a half single axle load with dual tire 40 KN was reduced to an equivalent load of 5 KN according to (1/3) scale to preserve similar pavement response across the laboratory model and the full-scale pavementDimensional analysis based on Buckingham Pi Theorem applied to a scaled pavement model to ensure that the 1/3 scale accelerated loading test (ALT) maintained geometric, material, and dynamic similarity with the full-scale pavement [28;29], where all linear dimensions were reduced by a factor of three. Stress and strain were preserved to replicate the mechanical response of the pavement model. Consequently, the applied load was scaled according to the square of the geometric scale as illustrated in Table 4.

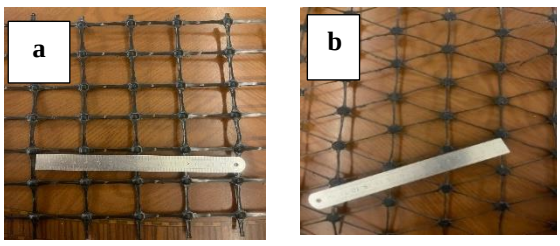

Fig. 2 (a) Biaxial Geogrid, (b) Triaxial Geogrid

A 3.0 kW hydraulic actuator was used to apply the load with a frequency of 0.21 Hz. This frequency is suitable for pavement response investigation since high-speed results in a reduction in critical pavement response, as the asphalt mixture becomes stiffer at higher frequencies [23-30].

Table 3. Specifications of PP Biaxial Geogrid (BX3030) and PP Triaxial Geogrid (TX150)

Item	PPX3030		TX150
	MD	TD	
Polymer	PP	PP	PP
Minimum Carbon Black %	2		2
Aperture Size mm	36	36	40*40*35
Rip Mid Distance mm	-	-	40
Tensile Strength kN/m	30	30	-
Tensile Strength @ 2% Strain kN/m	10.5	10.5	-
Tensile Strength @ 5% Strain kN/m	21	21	-
Radial Secant Stiffness at 2% Strain kN/m	-	-	185
Elongation %	13	13	13
Junction Efficiency %	93	93	96
Flexural Rigidity mg-cm	2,000,000		-
Aperture Stability m-N/deg	0.75		-

To examine other scenarios representing moderate pressure and high pressure, the load of 5

KN (480 KPa) was altered to achieve different loads and pressures. The additional load tested was 6.5 KN and 7.5 KN, corresponding to 560 KPa and 690 KPa pressure, respectively.

Table 4. Dimensional Scaling and Similitude Criteria

Parameter	Scaling Ratio	Justification
Length	1:3	Geometric Similarity
Contact Area	1:9	Derived from length scaling
Load	1:9	Stress preservation
Stress	1:1	Governing response
Strain	1:1	Directly measured
Temperature	1:1	Surface Pavement Temperature (35, 45)°C

4.2 Applied Load Simulation Setup

An accelerated load test assembly with pneumatic actuators and a rigid tire traveling in a unidirectional path that applied different contact pressures depending on the applied load from 400 kPa to 800 kPa was used to simulate tire pressure using a mechanical load frame, as depicted in Figure 3. This range represents the pressures found in typical commercial vehicles. The color-spray approach was used to experimentally estimate the actual tire–pavement contact area under the scaled load. To replicate actual tire-pavement interaction, the load contact area was computed as an equivalent rectangle in accordance with Huang Y. H. (2004); the dimensions were 8.5*12.3 cm, 8.9*13 cm, and 8.7*12.6 cm for 480 KPa, 560 KPa, and 690 KPa, respectively [1]. The loading configuration was created to replicate traffic-induced stress cycles by allowing for repeated loading at a regulated pressure.

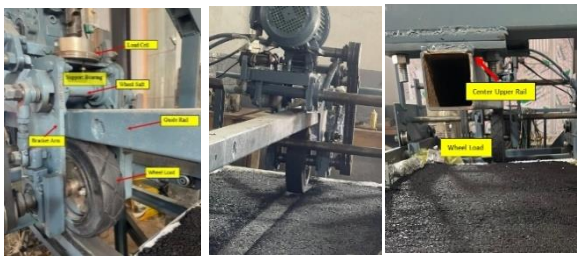

Fig. 3 Loading Setup

4.3 Load Sequence and Duration

Each pavement test section was tested by applying three sequential load levels of (5 KN, 6.5 KN, and 7.5 KN) using the same sample of pavement section. At the first and second stages, pavement test sections received 25,000 load cycles, while the final stage, with a load of 7.5 KN, continued until the rutting depth accumulated to 19.1 mm, which was adopted as the failure criterion. This sequential loading approach simulates the accumulation of field damage by subjecting the same pavement to successive overloading, thus capturing the deformation with the load magnitude increase. The total test duration for each section was approximately one month, depending on the section stiffness and reinforcement configuration.

4.4 Construction of the Scaled Model of Flexible Pavement

The scaled pavement test sections were built in layers within a rigid steel test box that measured 2.0 meters in length, 1.0 meters in width, and 0.70 meters in depth. To prevent the desired moisture content loss, a layer of plastic sheet was placed inside the container, and silicone was applied to the metal box's joint before placement of pavement layers. Based on the laboratory compaction test results, each layer was prepared and compacted to the desired density and moisture content. The water content for each subgrade lift was investigated before and after each accelerated test to ensure that the subgrade water content does not decrease or is minimized during the tests. The results show the water moisture content range between before the test was 26.130% and 26.245% within the different lifts and depths, and the moisture content after the test ranged between 26.141% and 26.259%, which varies within an acceptable range for a 26% moisture content value. The subgrade soil was compacted in successive lifts to achieve a target CBR value of 2.1%, thereby replicating weak subgrade conditions. The first lift was compacted manually by a hand tamper to a 10 cm thickness. The subsequent second and third lifts, each 20 cm thick, were compacted with a Robin Plate Compactor EY20, featuring a net weight of 100 kg and a 5.0 HP engine. A 3 cm-thick cork layer was mounted at the sides and on the bottom of the box under the subgrade to attenuate wave reflection from the lower base of the rigid metal box and to create a realistic boundary condition. The subbase, bituminous base courses, and bituminous wearing course were constructed and compacted to the specified density in a single layer, with thicknesses of 9.0 cm, 6.0 cm, and 5.0 cm, respectively, using the same plate vibratory compactor. The compaction process achieves a good representative for field compaction and interlocking between subbase aggregate and geogrids. For the reinforced sections, biaxial and triaxial geogrids were placed at the middle depth of the subbase layer and at the subbase-subgrade interface during construction with orientation control using laser alignment and 150 mm overlap to be anchored by nails at the corners of the test box. The pavement models of test sections are listed in Table 5.

Table 5. Pavement Test Sections

Sec. No.	Type of Geosynthetics	Location of Geosynthetics
Sec.1	Non	Control
Sec. 2	Triaxial Geogrid	Middle of Subbase Thickness
Sec. 3	Triaxial Geogrid	Subbase- Subgrade Interface
Sec. 4	Biaxial Geogrid	Middle of Subbase Thickness
Sec. 5	Biaxial Geogrid	Subbase- Subgrade Interface

4.5 Instrumentation and Data Collection System

A Foil-type strain gauge sensor of 50 mm length and a sensitivity range of ± 5000 με, a Linear Variable Differential Transformer (LVDT) from SONSEIK model TR50 series typically offers a length range of 50 mm, with micrometer-level resolution, and pancake-type load cell were used to measure the pavement's response under repeated wheel loads applied by device with a frequency of 0.21 Hz and a speed of 4.75 km/h (1.320 m/s), the device can handle about 750 load cycle applications per hour. The strain gauges were embedded above the base surface at the interface between the wearing surface and the base. Strain gauges typically produce a change in electrical resistance, which is converted into a voltage signal through a Wheatstone bridge circuit. This signal is then translated into strain. During each test sequence, real-strain, load, and displacement data were acquired with a sample rate of 50 readings per second, every 750 cycles or roughly every hour, and synced with the loading actuator using the data acquisition system and LabVIEW program.

The sensors were calibrated before every test using reference displacement and strain standards, and the calibration curves show a linear relation with a coefficient of correlation (R^2) of more than 0.999. Measurement of uncertainty was performed using a statistical approach by combining calibration and accuracy of the sensors using the root-sum-of-squares method, that is, by taking the square root of the sum of the individual errors [31]. The results revealed that the combined uncertainties at 95 % confidence level were ±0.08 mm for LVDT measurements, ±0.01 KN for the load cell, and ±3.3 μs for the strain gauges, confirming high repeatability in recording data.

All sensor data were processed using DIAdem 2022 software, as it was used to capture the measurement records during tests due to its capacity for handling large data, channel organization, and accurate statistical analysis and visualization. After importing the acceleration test data recorded from the LLES system, signal quality was first verified by examining the time series and identifying unstable readings resulting from wheel repositioning or the start or end of operation. After that, a low-pass smoothing filter was applied to remove noise, which is a common practice in pavement response measurement [32]. Neighbor-based averaging was used to correct abnormal spikes caused by cable motion or transient electrical interference, which were identified as statistical outliers exceeding ±2 standard deviations from the local mean [33]. The processed data were divided into individual loading cycles after cleaning, and the peak value for each measured variable in each cycle was extracted. This process guaranteed that the final data reflected the pavement structural response. Figure 4 represents the wave load form for 5 KN applied load.

5. RESULTS AND DISCUSSIONS

5.1 Measurement Repeatability

One replicate test was conducted for a trial test section for each load level to evaluate the consistency of measurements. Each section replicates the rutting depth and strain, which were measured cumulatively with load cycles. Repeatability for measurement was evaluated by the measurements for each section with the replication test for each section and load level by pointwise coefficient of variance and standard error [34]. The analysis results are shown in Table 6. Results show COV% less than 8 % in terms of rutting measurement and 0.645 in terms of strain, with standard error of 0.416 and 0.96, respectively, which indicates that the sections have consistent and repeatable application for rutting and strain measurements at multiple cycles.

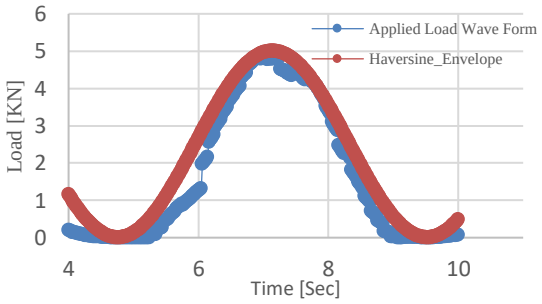

Fig. 4 Load Wave Form

Table 6. Reportability Statistics for Rutting and Strain Measurements

Variable	Mean	Sta. Dev.	C.V. (%)	Standard Error
Rutting	12.352	0.588	6.759	0.416
Strain	193.336	1.360	0.645	0.96

5.2 Permanent Deformation (Surface Rutting)

Five test sections have been tested under an accelerated load test application. The first load was 5 kN (480 kPa pressure), followed by 6.5 KN (560 kPa

pressure), and 7.5 KN (690 kPa pressure). Loading cycles were applied, 25000 cycles for the first and second load, and the third load was applied until the rutting depth reached 19.1 mm, following AASHTO criteria [35]. The geogrid reinforcement was used in two different locations, at the middle depth of the subbase layer and at the subbase and subgrade interface. Figure 5 compares the rutting depth for reinforced and unreinforced test sections. Generally, rutting depth increases with the increase in load cycles. All sections represent typical progress for rutting. In the initial cycles, there was a rapid increase, then a gradual, steady accumulation of plastic deformation. Similar behavior had been documented by several researchers [15-23]. In Figure 5, the rutting depth accumulation is characterized by two different deformation stages separated by a transition zone [36]. The initial densification phase, where the aggregate particles rearranged and air voids in the unbound layer decreased after 6000 to 10500 cycles. After approximately 18000 cycles for the control section and 125000 to 150000 cycles for the reinforced sections, the slope of the curve increases, indicating the beginning of the second phase of plastic deformation, where shear strain accumulates at the underlying pavement layers. The transition zone corresponds to the inflection point of each curve, representing the change from densification due to compaction to plastic deformation. In comparison to the control section, the reinforced sections showed a delayed transition, demonstrating that geogrid reinforcement minimized shear movement and improved the pavement sections' performance. Section 1, the control displayed the highest rutting rate, while sections 2, 3, 4, and 5 demonstrated better resistance to permanent deformation.

In terms of rutting depth reduction, using geogrid reduced rutting depth by 45% and 34 % for Triaxial and Biaxial geogrid at the subbase-subgrade interface, while reducing it by 30% and 23% for triaxial and biaxial geogrid at the middle depth of the subbase course. The utilization of triaxial geogrid was more effective than that of biaxial geogrid. This could be attributed to the highest radial secant stiffness at 2% strain for the triaxial geogrid, which enables it to distribute load effectively in three directions under different loading scenarios. Despite the superior performance of triaxial geogrid, the biaxial geogrid achieves good performance in rutting reduction. Rutting depth in flexible pavement is generally associated with lateral movement and shear deformation of base, subbase, and subgrade. The observed reduction in permeant deformation under the same loading conditions that are clearly shown in Figure 5 confirms that the geogrid restrained the lateral aggregate movement and limited shear deformation accumulation.

The Traffic Benefit Ratio (TBR) was computed based on the outcomes of the experimental work to evaluate the benefit of the geogrid reinforcement. TBR can be defined as the ratio between the specific cycle for reinforced sections (Nr) to reach a definite rutting depth the specific cycle for unreinforced sections (Nu) to achieve the same definite rutting depth, usually taken as 12.1mm, 19.1 mm, or 25.4 mm [37]. Increases in rutting depth result in higher TBR, suggesting that using a geosynthetic reinforcement within the pavement layer will likely improve performance [35]. TBR can be calculated from Equation (1):

$$TBR = \frac{N_r}{N_u} \quad (1)$$

Where:
N_r = Cycle for Reinforced Section
N_u = Cycle for Unreinforced Section

Table 6 displays the TBR for two different rutting depth criteria, 12.1 mm and 19.1 mm. The test findings show that employing the using the triaxial geogrid-reinforced at the middle depth of subbase course result in an estimated TBR of 3.3 at 12.1 mm rutting, corresponding to 231% improvement in load repetition and 3.5 at 19.1mm rutting for Section 2, corresponding to 251% while using the biaxial geogrid in the middle depth of subbase result in a TBR of 2.7 at 12.1 mm rutting, corresponding to 175 % and 3.0 at 19.1mm rutting for Section 4, corresponding to 198% improvement.

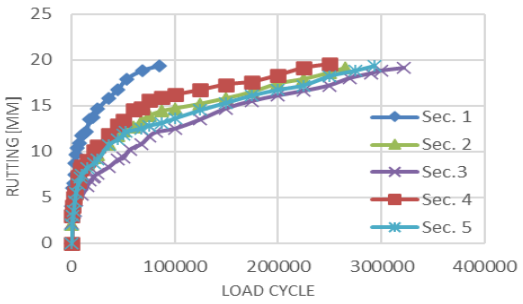

Fig. 5 Load Cycle relation with Permanent Deformation

In the same way, using the triaxial geogrid at the subbase-subgrade interface in section 3 results in TBR of 4.0 at 12.1 mm rutting, corresponding to 303 % improvement in load repetition, and 4.3 at 19.1mm rutting, corresponding to 326% improvement in load repetition. In contrast, using the biaxial geogrid at the subbase-subgrade interface results in a TBR of 3.7 at 12.1 mm rutting, corresponding to 273 % and 4.1 at 19.1 mm rutting for Section 5, corresponding to a 310 % improvement. These findings are illustrated in Table 7, which reveals the rising TBR at 19.1 mm rutting depth compared to 12.1 mm rutting depth, where the TBR

value increases when the rutting depth increases, resulting in the benefit of geogrids, which is confirmed by [38].

These results indicate that placing reinforcement within the subbase-subgrade interface is more effective in delaying rutting compared to locating it at the middle depth of the subbase layer because it contributes to reinforcing the weakest layer in the pavement section, which is the weak subgrade. Furthermore, the use of triaxial geogrid gives higher TRB values due to providing three-dimensional stiffness that enhances load distribution and a better confinement mechanism for the subbase. This implies the benefit of geogrid utilization to improve load distribution.

Nevertheless, TBR value for the scaled pavement model cannot be directly used to predict field pavement life, as they differ significantly according to subgrade strength, base or subbase thickness, geosynthetic type, loading condition, and rutting criteria. Conversely, TBR should be used in the Mechanistic-Empirical (M-E) design method through back calculation to an equivalent base or subbase modulus, structural number, or traffic capacity (ESAL) within a design method like AASHTO. It should be calibrated against full-scale field data [22; 37; 39;40].

Table 7. Traffic Benefit Ratio for Test Sections

Sec. No.	Rutting Depth = 12.1 mm		% Load Repetition Improvement	Rutting Depth = 19.1 mm		% Load Repetition Improvement
	Cycles	TBR		Cycles	TBR	
1	14,000	-----		75,600	-----	
2	46,300	3.3	231	265,000	3.5	251
3	56,500	4.0	303	322,150	4.3	326
4	38455	2.7	175	225,000	3.0	198
5	52150	3.7	273	310000	4.1	310

5.3 Tensile Strain at the Bottom of the Asphalt Surface Layer

All sections showed a rapid increase in tensile strain during the early loading stage, followed by a gradual accumulation at the second stage, after approximately 5000 cycles of loading, where the strain rate decreased significantly, as presented in Figure 6. From the figure, it can be seen that the control section exhibits the largest tensile strain during the load cycles, meaning a decrease in structural capacity. In contrast, geogrid reinforced sections for both triaxial and biaxial geogrid showed a significant reduction in tensile strain as presented in Figure 7. Where section 3 (TGI) presents the highest average reduction value 84% followed by section 5 (BGI) with a reduction percent of 78%, both sections reinforced at the subbase-subgrade interface. On the other hand, section 2 (TGM) exhibits 62%, and section 4 (BGM) shows the lowest percent reduction of 49%. This could be due to the geogrid reinforcement location. When placed at the mid-depth of the subbase, mainly mobilizes interlock and lateral confinement and improves the stiffness of the layer itself [41], while placement of geogrid at the subbase-subgrade interface acts where vertical compressive and shear strain in the weak subgrade are maximum result in direct restraint of shear deformation and strain accumulation that provides better performance [42].

These reductions indicate an increase in the haul pavement structural stiffness due to geogrid confinement of subbase aggregate, resulting in a reduction in deformation of the wearing surface layer, which is consistent with previous studies, which stated that geogrid reinforcement could improve pavement performance [6-23]. The simultaneous reduction in rutting depth and tensile strain implied that the geogrid reinforcement improved load transfer mechanisms by redistributing the wheel load on a larger area and increasing subbase aggregate confinement that minimizes and delays structural failure.

5.4 Load Sensitivity Analysis

A load sensitivity analysis was conducted to evaluate which reinforcement configuration exhibits the lowest sensitivity to load change. The analysis includes determining the values of the increase in strain at the last 25000 cycles for each load level of the test sections and averaging them. Secondly, find the sensitivity for every KN increase in load by dividing the average increase value by the increment of load raised from 5 KN to 7.5 KN, which is a 2.5 increment. The last step calculates the sensitivity index relative to the control (unreinforced section) by dividing the sensitivity for each section in (μs/KN) by the sensitivity in (μs/KN) for the control section.

The results are shown in Table 8 and Figure 7. The lower sensitivity index reflects a better load distribution and a more stable performance indicator. Section 3 (TGI) and Section 5 (BGI) present the lowest sensitivity index of 0.30 and 0.35, respectively, while Sections 2 and 4 show higher indices of 0.74 and 0.7 relative to the control section. These results further confirm that triaxial geogrid sections offer superior structural reinforcement, while the interface between subbase and subgrade is the optimal reinforcement location. There is a nonlinear relation between load and tensile strain (a power relation) as shown in Figure 7, with R^2 ranging from 0.808 to 0.999.

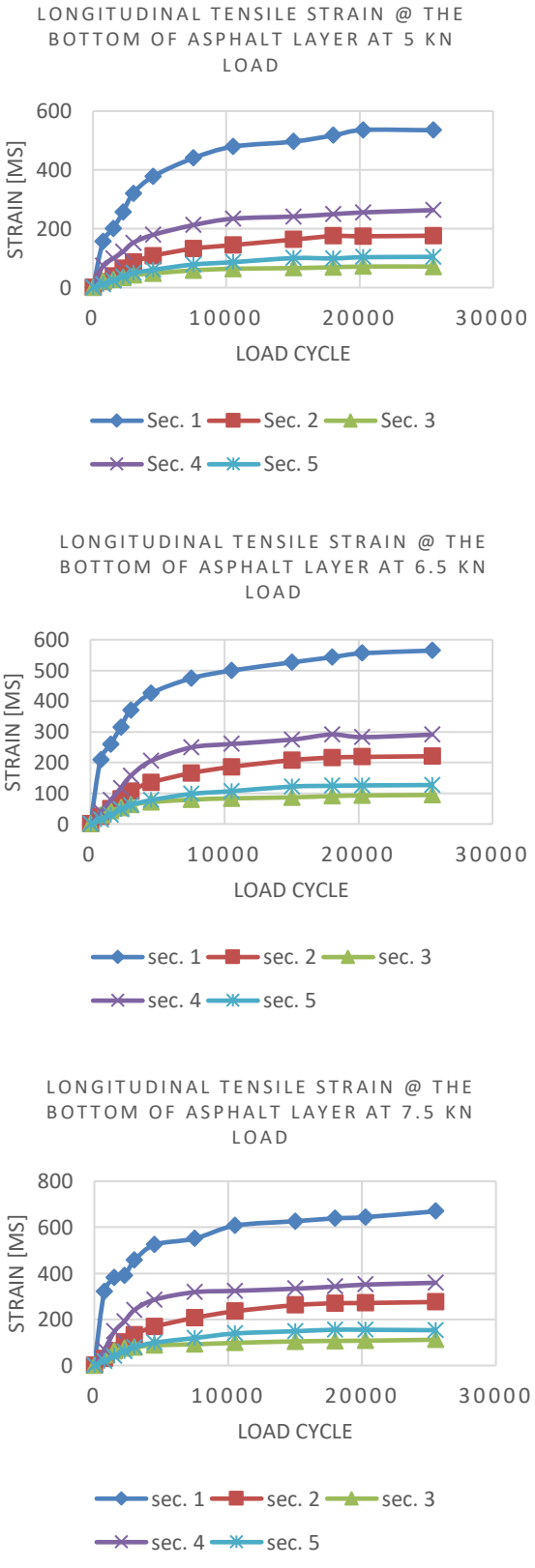

Fig. 6 Tensile Strain at the Bottom of the Asphalt Layer

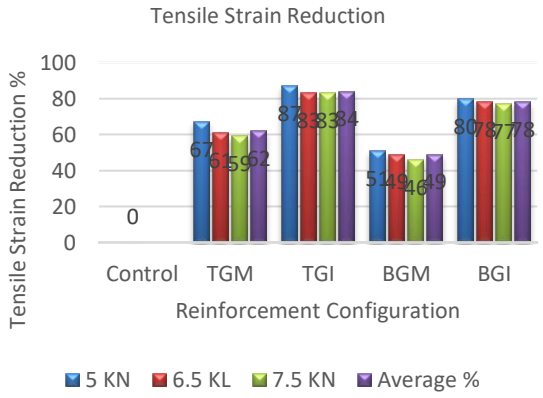

Fig. 7 Tensile Strain Reduction Percent

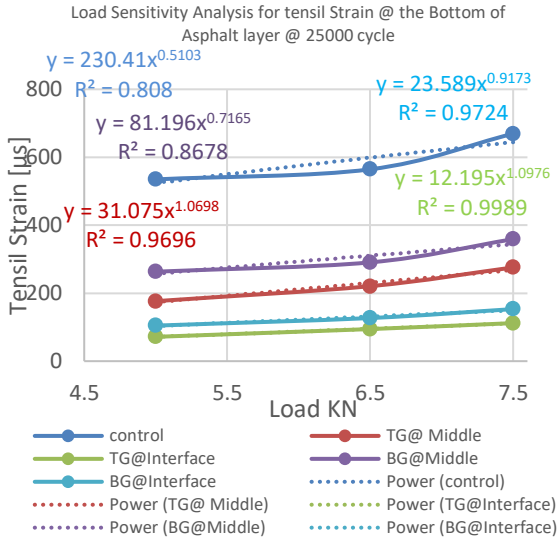

Fig. 8 Load Sensitivity Analysis for Tensile Strain at the Bottom of the Asphalt layer at 25000 cycles

Table 8. Load Sensitivity Analysis Results

Sect. No.	Reinforcement Configuration	Strain Increase µs	Sensitivity (µs/KN)	Sensitivity Index Relative to Control Section
1	control	135	54	1.00
2	TGM	99	40	0.74
3	TGI	41	16	0.30
4	BGM	95	38	0.70
5	BGI	48	19	0.35

6. CONCLUSION

The Key finding from the current study can be summarized in the following points:

1- Load increase results in a significant increase in tensile strain at the bottom of the asphalt layer.

2- Geogrid reinforcement significantly improved pavement performance by reducing surface rutting and tensile strain at the bottom of the asphalt layer.

3- Triaxial geogrid demonstrates superior performance in both rutting resistance and tensile strain reduction compared to biaxial geogrid, with more benefit achieved by placing it at the interface of subbase-subgrade.

4- Triaxial geogrid reduced rutting depth by an average of 45% when placed at the subbase subgrade interface and 30 % when placed at the middle depth of the subbase course.

5- Flexible pavement reinforced with geogrid significantly reduces tensile strain at the bottom of the asphalt layer, with percentages of 49% to 84% depending on reinforcement configuration.

6- Biaxial geogrid still provides good reinforcement relative to unreinforced sections, especially when placed at the subbase-subgrade interface.

7- Reinforcement by triaxial geogrid placement at the subbase subgrade interface achieves TBR of 4.0 to 4.3, corresponding to 303-326% improvement in load repetition at 12.1 mm and 19.1 mm rutting depth.

8- Load sensitivity analysis revealed that the triaxial geogrid at the subbase-subgrade interface had the lowest sensitivity index of 0.30, compared to 1.00 for the control (unreinforced section). This indicates a 70% reduction in sensitivity to load increase and superior load distribution.

7. ACKNOWLEDGEMENT

The author gratefully acknowledges the support provided by the College of Civil Engineering, University of Technology - Iraq, for facilitating the experimental work and providing the laboratory resources. Sincere appreciation is extended to the supervisor, Prof. Dr. Hasan H. J., for valuable guidance and constructive suggestions throughout the research.

8. REFERENCES

1. Huang Y.H., Pavement analysis and design, Upper Saddle River, NJ: Pearson/Prentice Hall, 2004, pp. 401-409.
2. Abd Ali N.S., Joni H.H. and Al-Rubaee R.H. Effect of asphalt modified with waste engine oil on the durability properties of hot asphalt mixtures with reclaimed asphalt pavement. Open Engineering, 14(1), 2024, p.20220529. https://doi.org/10.1515/eng-2022-0529
3. Menkash O.A., Joni, H.H. and Nsaif M. An experimental study on the tensile properties of reinforced asphalt pavement. Open Engineering, 14(1), 2024, p.20220591. https://doi.org/10.1515/eng-2022-0591
4. Giroud J.P. and Han J. Design method for geogrid-reinforced unpaved roads. I. Development of design method. Journal of geotechnical and geoenvironmental engineering, 130(8), 2004, pp.775-786. doi.org/10.1061/(ASCE)10900241(2004)130:8(775)
5. Jasim A.F., Fattah M.Y., Al-Saadi I.F. and Abbas, A.S. Geogrid reinforcement optimal location under different tire contact stress assumptions. International Journal of Pavement Research and Technology, 14(3), 2021, pp.357-365. doi.org/10.1007/s42947-020-0145-6
6. Al-Qadi I.L., Yoo P.J., Elseifi M.A. and Janajreh I. Effects of Tire Configurations on Pavement Damage. Journal of the Association of Asphalt Paving Technologists, 74(1): 921-61, 2005.
7. Gunasekara Jayalath C.P., Gallage C., Dhanasekar M., Dareeju B., Ramanujam J. and Lee J. Pavement model tests to investigate the effects of geogrid as subgrade reinforcement. In Proceedings of the 12th Australian and New Zealand young geotechnical professionals conference, Australian Geomechanics Society, 2018, pp. 1-8.
8. Nazzal M.D. Laboratory characterization and numerical modeling of geogrid reinforced bases in flexible pavements. Louisiana State University and Agricultural & Mechanical College, 2007. https://digitalcommons.lsu.edu/gradschool_dissertations
9. Abu-Farsakh M. and Nazzal M. Evaluation of the Base/Subgrade Soil under Repeated Loading: Phase 1–Laboratory Testing and Numerical Modeling of Geogrid Reinforced Bases in Flexible Pavement (No. FHWA/LA. 09/450), 2009. https://rosap.ntl.bts.gov/view/dot/18256/dot_18256_DS
10. Sami D.A., Hameed H. and Hilal M.M., Effect of reinforced asphalt pavement layers with geotextile under dynamic load. In AIP Conference Proceedings, AIP Publishing LLC, 3105(1), 2024, p. 050063. doi.org/10.1063/5.0212903
11. Ibrahim S.F., Ahmed N.G. and Mohammed D.E., Effect of Reinforcement on Improve Surface Pavement for Weak Subgrade Conditions. International Journal, 11(23), 2016, pp.2188-2193. https://geomatejournal.com/geomate/article/view/2530
12. Hussein M., Fattah M. and Hilal M., Dynamic Behavior of Pavement Layers on Sand Subgrade. Engineering and Technology Journal, 39(12), 2021, pp.1760-1770. doi.org/10.30684/etj.v39i12.1770
13. Zornberg J.G. Advances in the use of geosynthetics in pavement projects. In Keynote

lecture, proceedings of the 2nd Iberic conference on geosynthetics, Geosintec Iberia, 2015, pp. 07-08.
14. Qian Y., Han J., Pokharel S.K. and Parsons R.L., Experimental study on triaxial geogrid-reinforced bases over weak subgrade under cyclic loading. In GeoFlorida 2010: Advances in Analysis, Modeling & Design, 2010, pp. 1208-1216. doi.org/10.1061/41095(365)120
15. Jersey S.R., Tingle J.S., Norwood G.J., Kwon J. and Wayne M., Full-scale evaluation of geogrid-reinforced thin flexible pavements. Transportation research record, 2310(1), 2012, pp.61-71. doi.org/10.3141/2310-07
16. Abu-Farsakh M.Y., Gu J., Voyiadjis G.Z. and Chen Q. Mechanistic–empirical analysis of the results of finite element analysis on flexible pavement with geogrid base reinforcement. International Journal of Pavement Engineering, 15(9), 2014, pp.786-798. doi.org/10.1080/10298436.2014.893315
17. Ferrotti G., Canestrari F., Virgili A. and Grilli A. A., strategic laboratory approach for the performance investigation of geogrids in flexible pavements. Construction and Building Materials, 25(5), 2011, pp.2343-2348. doi.org/10.1016/j.conbuildmat.2010.11.032
18. Ghafoori N. and Sharbaf M., Evaluation of triaxial geogrids for reduction of base thickness in flexible pavements. Bituminous Mixtures and Pavements VI, 2015, p.141. http://worldcat.org/isbn/9781138028661
19. Kwon J. and Tutumluer E., Geogrid base reinforcement with aggregate interlock and modeling of associated stiffness enhancement in mechanistic pavement analysis. Transportation research record, 2116(1), 2009, pp.85-95. doi.org/10.3141/2116-12
20. Kim M. and Lee J.H., Effects of geogrid reinforcement in low volume flexible pavement. Journal of Civil Engineering and Management, 19 (sup1), 2013, pp. S14-S22. doi:10.3846/13923730.2013.793606
21. Huang B., Gong H. and Shu X., Evaluation of Geosynthetics Reinforcement in Flexible Pavement Structures Using Accelerated Pavement Testing (No. RES 2013-30), 2018. https://rosap.ntl.bts.gov/view/dot/55042
22. Baadiga R., Balunaini U., Saride S. and Madhav M.R., Effect of geogrid type and subgrade strength on the traffic benefit ratio of flexible pavements. Transportation Infrastructure Geotechnology, 10 (2), 2023, pp.180-210. doi.org/10.1007/s40515-021-00203-5
23. Al-Qadi I.L., Dessouky S., Tutumluer E. and Kwon J., Geogrid mechanism in low-volume flexible pavements: accelerated testing of full-scale heavily instrumented pavement sections. International Journal of Pavement Engineering, 12(02), 2011, pp.121-135. doi.org/10.1080/10298436.2010.535534
24. Valašková V., Vlček J. and Papán D., Determination of the Small-Scale Physical Model Parameters of Pavement Structure. Sustainability, 12(22), 2020, p. 9637. doi.org/10.3390/su12229637
25. Perkins S.W., Ismeik M.A., Synthesis and Evaluation of Geosynthetic-Reinforced Base Layers in Flexible Pavements- Part I. Geosynth Int. 4(6), 1997, pp. 549–604.
26. Rasheed R.M., Moghal A.A.B., Basha B.M. and Almajed A., Effect of Chitosan and Casein on the CBR behavior of silty clay for low volume roads: Reliability-based design optimization approach. Construction and Building Materials, 473, 2025, p.141014. doi.org/10.1016/j.conbuildmat.2025.141014
27. Han B., Ling J., Shu X., Gong H., and Huang B., Laboratory investigation of particle size effects on the shear behavior of aggregate-geogrid interface. Construction and Building Materials, 158, 2018, pp.1015-1025. doi.org/10.1016/j.conbuildmat.2017.10.045
28. Buckingham E., On Physically Similar Systems; Illustrations of the Use of Dimensional Equations. Physical Review, 4(4),1914, pp.345-376. doi.org/10.1103/PhysRev.4.34
29. Tolun M., Efficiency of Dimensional Analysis in Predicting Compression Load–Settlement Relationship of Soft Clay Under a Rigid Foundation. Applied Sciences, 14(23), 2024, p.11252. doi.org/10.3390/app142311252
30. Garg N. and Hayhoe G.F., Asphalt concrete strain responses at high loads and low speeds at the national airport pavement test facility (NAPTF). In Advancing airfield pavements, 2001, pp. 1-14. https://doi.org/10.1061/40579(271)1.
31. Bevington P.R., Robinson D.K., Blair J.M., Mallinckrodt A.J., and McKay S., Data Reduction and Error Analysis for the Physical Sciences. Computers in Physics, 7(4), 1993, pp.415-416.
32. Daniewicz S., Smoothing and differentiating load-displacement data using a low-pass filter for improved crack opening load estimates. Fatigue & fracture of engineering materials & structures, 22(4), 1999, pp.273-279.
33. Yang J., Rahardja S., and Fränti P., Outlier detection: How to threshold outlier scores?. In Proceedings of the international conference on artificial intelligence, information processing and cloud computing, 2019, pp. 1-6. doi.org/10.1145/3371425.3371427
34. ISO. I., and OIML B., Guide to the Expression of Uncertainty in Measurement. Madrid, Spain: Aenor, 1993.
35. American Association of State Highway and Transportation Officials (AASHTO). Guide for

Design of Pavement Structures. Washington (DC): AASHTO; 1993.
36. Joumblat R., Al Basiouni Al Masri Z., Al Khateeb G., Elkordi A., El Tallis A.R., and Absi J., State-of-the-art review on permanent deformation characterization of asphalt concrete pavements. Sustainability, 15(2), 2023, p.1166. doi.org/10.3390/su15021166
37. Zadehmohamad M., Luo N., Abu-Farsakh M., and Voyiadjis G., Evaluating long-term benefits of geosynthetics in flexible pavements built over weak subgrades by finite element and Mechanistic-Empirical analyses. Geotextiles and Geomembranes, 50(3), 2022, pp.455-469. doi.org/120.1016/j.geotexmem.2022.01.004
38. Wimalasena K., and Jayalath C.P.G., Effect of geogrid reinforcement in weak subgrades. GEOMATE Journal, 18(65), 2020, pp.140-146. doi.org/10.21660/2020.65.90377
39. Abu-Farsakh M., Zadehmohamad M., and Voyiadjis G.Z., Incorporating the Benefits of Geosynthetic into MEPDG. Infrastructures, 8(2), 2023, p.35. doi.org/10.3390/infrastructures8020035
40. Sa'adi A.H.M.A., Al-Maimuri N.M.L. and Omar al-mamany D.A., Effect of geotextile reinforcement on flexible pavement roads. Engineering and Technology Journal, 31, 2013, pp.299-315. doi.org/10.30684/etj.2013.83801
41. Jebur F.F., Fattah M.Y. and Abduljabbar A.S., Function and application of geogrid in flexible pavement under dynamic load. Engineering and Technology Journal, 39(08), 2021, pp.1231-1241. doi.org/10.30684/etj.v39i8.1771
42. Banyhussan Q.S., and Kadhum A.J., Performance of Reinforced Subbase Materials by Geogrid as a Base Layer Under Weak Subgrade. In E3S Web of Conferences, Vol. 427, 2023, p. 03008. EDP Sciences. doi.org/10.1051/e3sconf/202342703008

Copyright © Int. J. of GEOMATE All rights reserved, including making copies, unless permission is obtained from the copyright proprietors.